JACS
JOURNAL OF THE AMERICAN CHEMICAL SOCIETY
Article
pubs.acs.org/JACS

Ligand Exchange Governs the Crystal Structures in Binary Nanocrystal Superlattices

Jingjing Wei,[†,‡] Nicolas Schaeffer,[†,‡] and Marie-Paule Pileni*[,†,‡,§]

[†]Sorbonne Universités, UPMC Université Paris 06, UMR 8233, MONARIS, F-75005 Paris, France
[‡]CNRS, UMR 8233, MONARIS, F-75005 Paris, France
[§]CEA/IRAMIS, CEA Saclay, 91191 Gif-sur-Yvette, France

Supporting Information

ABSTRACT: The surface chemistry in colloidal nanocrystals on the final crystalline structure of binary superlattices produced by self-assembly of two sets of nanocrystals is hereby demonstrated. By mixing nanocrystals having two different sizes and the same coating agent, oleylamine (OAM), the binary nanocrystal superlattices that are produced, such as NaCl, AlB_2, $NaZn_{13}$, and $MgZn_2$, are well in agreement with the crystalline structures predicted by the hard-sphere model, their formation being purely driven by entropic forces. By opposition, when large and small nanocrystals are coated with two different ligands [OAM and dodecanethiol (DDT), respectively] while keeping all other experimental conditions unchanged, the final binary structures markedly change and various structures with lower packing densities, such as Cu_3Au, CaB_6, and quasicrystals, are observed. This effect of the nanocrystals' coating agents could also be extended to other binary systems, such as Ag−Au and $CoFe_2O_4$−Ag supracrystalline binary lattices. In order to understand this effect, a mechanism based on ligand exchange process is proposed. Ligand exchange mechanism is believed to affect the thermodynamics in the formation of binary systems composed of two sets of nanocrystals with different sizes and bearing two different coating agents. Hence, the formation of binary superlattices with lower packing densities may be favored kinetically because the required energetic penalty is smaller than that of a denser structure.

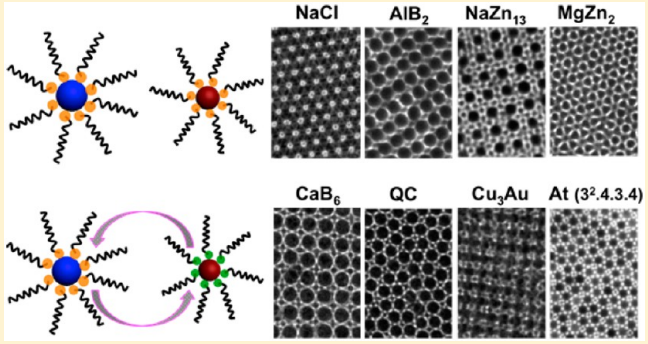

INTRODUCTION

The self-assembly of micrometer-sized colloids has been intensively studied, and it has been found that their phase behavior is determined by minimizing the system's free energy $F = U - TS$ or, since those colloids are forbidden to interpenetrate and the thermal energy U is a constant, by maximizing the entropy S.[1−5] When scaling the size of this type of system down to the nanoscale while considering flexible organic molecules on the surface of the nanocrystals, the assembly process is accompanied by effective control over the interactions between the nanocrystals and all entropic forces.[6−8] The interactions between nanocrystals can be described by a soft-sphere model which assumes isotropic nanocrystal interaction potentials. Built on this, the formation of close-packed arrays can be predicted.[9,10] However, the electrical charges induced by the coating agents and their surface coverage introduce important perturbations that can lead to the formation of superlattices with lower packing densities.[11,12] Although advances have been made using a variety of electrostatic forces, covalent or noncovalent molecular interactions to control the crystal structures, it remains a challenge to use spontaneous self-assembly to predict the phase structures composed of two different types of building blocks, namely, binary nanocrystal superlattices.[13]

A variety of crystal phases in binary nanocrystal superlattices have been built from nanocrystals of semiconductors, metals and oxides, and the prediction of the crystal structures mainly relies on the space-filling principles. At the exception of the well-known crystal structures analogous to NaCl, AlB_2, $NaZn_{13}$, and laves phases observed in binary microcolloid systems,[14−16] crystal structures such as CuAu-type, Cu_3Au-type, Fe_4C-type, and CaB_6-type as well as quasicrystalline order have also been discovered in binary nanocrystal superlattices.[17−20] The emergence of these binary nanocrystal superlattices cannot be simply predicted from the hard-sphere models and requires further study.

In the present work, colloidal binary nanocrystal mixtures containing two distinct types of nanocrystals with either the same or two different surface coating agents are used to grow binary nanocrystal superlattices, respectively. A systematic study on binary nanocrystal superlattices made of Ag−Ag binary mixtures with two distinct nanocrystal sizes is described in order to shed light on the effect of surface capping on the structure control of binary nanocrystal superlattices. Further-

Received: September 22, 2015
Published: November 9, 2015

DOI: 10.1021/jacs.5b09959
J. Am. Chem. Soc. 2015, 137, 14773−14784

Table 1. Parameters of the Nanocrystals Used as Building Blocks for the Growth of Binary Superlattices in the Present Work

nanocrystal@coating agent	diameter/nm	size distribution σ/%	D_{eff}/nm[a]	D_{eff} distribution/%[a]
Ag@OAM[b]	2.9	8	5.9	7
	3.7	6	6.3	6
	5.5	7	8.0	6
	7.5	8	9.9	7
	8.2	7	10.8	5
	9.6	7	12.1	6
	11.9	6	14.3	5
Ag@DDT[c]	4.0	9	6.0	9
Au@DDT[c]	4.0	8	5.9	6
$CoFe_2O_4$@OA[d]	12.0	5	14.0	6

[a]D_{eff} is the center-to-center distance measured from TEM images by counting about 500 nanocrystals. [b]OAM: oleylamine. [c]DDT: dodecanethiol. [d]OA: oleic acid.

more, we show that this effect can be extended to other binary systems, such as Ag−Au and $CoFe_2O_4$−Ag.

RESULTS AND DISCUSSION

Series of nanocrystals differing by their compositions, coating agents, diameters, all characterized by low size distributions, were used to produce binary nanocrystal superlattices. These include Ag, Au, and $CoFe_2O_4$ nanocrystals, their coating agents varying from oleylamine (OAM), to oleic acid (OA) and dodecanethiol (DDT). The diameters (D) of the nanocrystals range from 2.9 to 12 nm for Ag nanocrystals; Au and $CoFe_2O_4$ nanocrystals are 4 and 12 nm in diameter, respectively. The various diameters and the corresponding size distributions (σ) of these nanocrystals are shown in Table 1 and Figures S1 and S2 (TEM images and size distribution histograms, Supporting Information).

In a typical experiment, two colloidal solutions containing either small (S) or large (L) hydrophobic nanocrystals were dispersed in toluene. The native nanocrystal concentration was fixed to $[\text{nanocrystals}]_S = [\text{nanocrystals}]_L = 1 \times 10^{-6}$ M. The relative ratios between small and large nanocrystals were determined by varying the relative volume of the two colloidal solutions, and this value was tuned from 2 to 10. The superlattices were prepared by evaporating 40 μL of mixed colloidal solution deposited on a transmission electron microscopy (TEM) grid covered by a thin carbon film and placed at the bottom of the beaker under slow N_2 flow protection at 35 °C. The complete evaporation of carrier solvent occurs after ∼4 h under this condition.

The effective nanocrystal diameter, D_{eff}, is defined as the center-to-center distance between nanocrystals self-ordered in a compact hexagonal network, i.e., as the sum of the inorganic core diameter and twice the thickness of the organic ligand layer thickness. The D_{eff} values of the nanocrystals hereby studied are given in Table 1, and the corresponding size histograms are presented in Figure S3 (Supporting Information). The effective diameter ratio, γ_{eff}, is defined as $\gamma_{eff} = (D_{eff})_S/(D_{eff})_L$ and plays a determining role during the assembly of binary mixtures.[21] By depositing the binary mixture on the substrate, the system is expected to adopt the crystal structure corresponding to the most efficient space-filling system and reach a maximum packing density ρ for a given ratio of the sphere radii γ.[4,22,23] Different binary structures are produced depending on the γ values. Here, a large variety of nanocrystals differing by their nature (Ag, Au, $CoFe_2O_4$) and/or coating agents are used; the binary crystalline structures produced with those nanocrystals are summarized in Tables 2 and 3. When the stoichiometry of the final crystalline structure differs from that of the two types of nanocrystals used to produce it, the excess nanocrystals self-assemble into single-component superlattices (SCS) or amorphous phases (Am). For example, for similar amounts of small and large nanocrystals and for a γ value leading to a $NaZn_{13}$ structure, the expected binary superlattices are produced and the large nanocrystals not involved in this binary structure self-assemble into another crystalline structure (fcc, hcp, or bcc). In this case, an estimate of the relative amount of these phases (SCS and Am) was statistically measured from the surface area coverage on the TEM grids; those values are given in Tables 2 and 3.

Binary mixtures of Ag nanocrystals differing by their diameters and coated with oleylamine (OAM), referred to as Ag@OAM hereafter, are first considered. The relative concentration ratio $[Ag]_S/[Ag]_L$ was fixed to 4. The large nanocrystals have an average diameter of 11.9 nm with a size distribution of 6%, whereas the diameter and size distribution of the small nanocrystals are 2.9 nm and 8%, respectively, with γ_{eff} = 0.42. Figure 1a shows that the smaller Ag@OAM nanocrystals are located into the vacancies between the larger nanocrystals, resulting in a binary structure that is analogous to that of NaCl in atomic solids (space group $Fm\bar{3}m$).[24] TEM images show typical (111) crystal planes of NaCl-type binary superlattices with the corresponding crystal model shown in Figure 1a (insets). Keeping the large 11.9 nm nanocrystals while replacing the smaller ones with 3.7 nm induces the γ_{eff} value to increase to 0.44; in this case, similar features are obtained with the formation of NaCl-type binary structures (Figure 1b and Figure S4, Supporting Information). An increase of the γ_{eff} value to 0.52 obtained by varying the average diameter of larger nanocrystals to 9.6 nm while keeping the same small ones (3.7 nm) led to the appearance of AlB_2-type structures, as shown on the TEM images presented in Figure 1c.[13] Another further increase of γ_{eff} value to 0.55 and 0.58 by using large (8.2 nm) and small (2.9 and 3.7 nm) nanocrystals, respectively (Figure 1, parts d and e), still produced AlB_2-type structures without any detectable single-component superlattices (Table 2). However, another $NaZn_{13}$-type binary structure is also observed in the case of γ_{eff} = 0.58 (Figure 1f). This $NaZn_{13}$-type binary structure was still observed after another increase of γ_{eff} to 0.64 (7.5 and 3.7 nm nanocrystals), as shown in Figure 1g. Finally, increasing the γ_{eff} value to 0.79 (5.5 and 3.7 nm nanocrystals) and 0.81 (7.5 and 5.5 nm nanocrystals) led to the formation of ordered $MgZn_2$-type binary structures (Figure 1, parts h and i). For all binary systems made of nanocrystals bearing the same coating

DOI: 10.1021/jacs.5b09959
J. Am. Chem. Soc. 2015, 137, 14773−14784

Table 2. Influence of the Nanocrystals Concentration Ratios $[Ag]_S/[Ag]_L$ and Effective Diameter Ratios γ_{eff} on the Crystal Structures of Binary Superlattices Assembled from Bidisperse Ag@OAM Nanocrystals[a]

nanocrystal ratios $[Ag]_S/[Ag]_L$			2:1	4:1	10:1
Ag_L size/nm	Ag_S size/nm	effective size ratio γ_{eff}			
11.9	2.9	~0.42	NaCl	NaCl + SCS* (15–25%)	NaCl + SCS* (20–45%)
11.9	3.7	~0.44	NaCl	NaCl + SCS* (25–35%)	NaCl + SCS* (30–50%)
9.6	3.7	~0.52	AlB_2	SCS* (5–10%) + AlB_2	SCS* (20–30%) + AlB_2
8.2	2.9	~0.55	AlB_2	AlB_2	AlB_2 + SCS* (25–35%)
8.2	3.7	~0.58	AlB_2	AlB_2 + $NaZn_{13}$	$NaZn_{13}$
7.5	3.7	~0.64	$NaZn_{13}$ + $Am^{\times}$ (40–60%)	$NaZn_{13}$ + $Am^{\times}$ (30–50%)	$NaZn_{13}$ + $Am^{\times}$ (5–10%)
5.5	3.7	~0.79	$MgZn_2$ + $Am^{\times}$ (5–10%)	$MgZn_2$ + SCS* (10–25%) + $Am^{\times}$ (10–30%)	SCS* (10–40%) + $Am^{\times}$ (10–40%)
7.5	5.5	~0.81	$MgZn_2$	$MgZn_2$ + SCS* (15–30%)	$MgZn_2$ + SCS* (30–50%) + $Am^{\times}$ (5–10%)

[a]Note: SCS*, single-component nanocrystal superlattices; $Am^{\times}$, amorphous films; the data in the bracket is the percentage SCS and Am phases of the surface area coverage in the TEM grids.

agent (OAM), the crystalline domains are relatively large and reach several micrometers (Figure S5, Supporting Information). Previous studies showed that the change of the relative ratios of two colloidal solutions induces phase transformation in binary nanocrystal superlattices.[23] Hence, the relative volume of colloidal solutions containing either small or large Ag@OAM nanocrystals was modulated, and the results summarized in Table 2 show that similar data are produced with $[Ag]_S/[Ag]_L$ = 2 and 10 by comparison with $[Ag]_S/[Ag]_L$ = 4 (see Figures S6 and S7 for TEM images, Supporting Information).

Figure 2a shows the phase diagram of the binary nanocrystal superlattices made of Ag nanocrystals differing by their sizes but coated with the same ligand (OAM). A clear sequential structural evolution of binary nanocrystal superlattices from NaCl, AlB_2, $NaZn_{13}$, to $MgZn_2$ with the increase of γ_{eff} value can be observed. This sequence is in accordance with the phase diagrams determined from free energy calculations in computer simulations for binary mixtures of hard spheres (see Figure 2b).[16] In those simulations for hard-sphere models, the self-organization of hard spheres into binary structures is driven purely by entropic forces. During the condensation of the colloidal hard spheres, the entropic variation is positive and reaches a maximum when the ordering has the highest packing density. To date, available theoretical predictions can be made based on the calculation of free energy of entropy contribution, and it has been pointed out that NaCl, AlB_2, and $NaZn_{13}$ are stable in the range of $0.414 \leq \gamma \leq 0.45$, $0.45 \leq \gamma \leq 0.61$, and $0.54 \leq \gamma \leq 0.625$, respectively.[14] Laves phases ($MgZn_2$, $MgCu_2$, $MgNi_2$) are stable in the range of $0.76 \leq \gamma \leq 0.84$.[14] These data confirm that the hard-sphere model is also valid for binary nanocrystal mixtures with the same coating agent. Consequently, the crystal structures of binary superlattices made from binary mixtures with the same coating agent can be predicted from the calculated phase diagrams based on a hard-sphere model.

The influence of the coating agent on the formation of binary structures was then investigated in order to verify if the hard-sphere model can still be applied for binary mixtures containing two types of nanocrystals bearing different coatings agents. First, we considered the binary mixture in which 11.9 nm Ag@OAM nanocrystals were used as large nanocrystals, whereas small nanocrystals were replaced by 4.0 nm Ag nanocrystals coated with dodecanethiol (Ag@DDT) (Figure 3a). This corresponds to γ_{eff} value of ~0.42. All other experimental conditions remained unchanged, and $[Ag]_S/[Ag]_L$ was kept equal to 4. Figure 3b shows long-range ordered crystal domains up to micrometer scale of CaB_6-type superlattices, in which six small Ag nanocrystals form the octahedral cluster, this octahedral cluster being surrounded by the simple cubic-packed large Ag nanocrystals, and matching well with the corresponding crystal model (inset in Figure 3b). This corresponds to the (100) plane of the CaB_6 phase. This is remarkably different from the NaCl-type structure observed for superlattices made of two types of nanocrystals with sizes similar to those used here (similar γ_{eff} value) but both bearing the same coating agents (OAM). Here, the NaCl-type structure is not observed any more. In some regions of the TEM grid, it is observed that the octahedral shape with six small Ag nanocrystals and single small Ag nanocrystals are separated by the large Ag nanocrystals in a random manner (Figure 3d). For those structures, the fast Fourier transform (FFT) pattern shows a 12-fold symmetry, revealing its dodecagonal quasicrystalline (QC) order, which is in agreement with the

DOI: 10.1021/jacs.5b09959
J. Am. Chem. Soc. 2015, 137, 14773−14784

Table 3. Influence of the Nanocrystals Concentration Ratios $[Ag]_S/[Ag]_L$ and Effective Diameter Ratios γ_{eff} on the Crystal Structures of Binary Superlattices Assembled of Ag Nanocrystals Differing by Their Sizes and Coating Agents (Ag@OAM and Ag@DDT)[a]

nanocrystal ratios $[Ag_S]/[Ag_L]$				
Ag_L size/nm	effective size ratio γ	2:1	4:1	10:1
11.9	~0.42	quasicrystal + CaB_6 + $Am^{\times}$ (10−30%)	CaB_6 + quasicrystal	CaB_6 + SCS* (20−40%)
9.6	~0.50	NaCl + AlB_2 + Cu_3Au	AlB_2 + Cu_3Au	AlB_2 + Cu_3Au + $NaZn_{13}$
8.2	~0.56	AlB_2 + $NaZn_{13}$	AlB_2 + $NaZn_{13}$ + Cu_3Au	$NaZn_{13}$
7.4	~0.61	AlB_2 + $NaZn_{13}$	AlB_2 + Cu_3Au	$Am^{\times}$ (30−60%) + SCS* (10−40%)
5.5	~0.75	$Am^{\times}$ (50−70%)	$Am^{\times}$ (50−80%)	$Am^{\times}$ (50−80%)

[a]Note: SCS*, single-component nanocrystal superlattices; $Am^{\times}$, amorphous films; the data in the bracket is the percentage SCS and Am phases of the surface area coverage in the TEM grids.

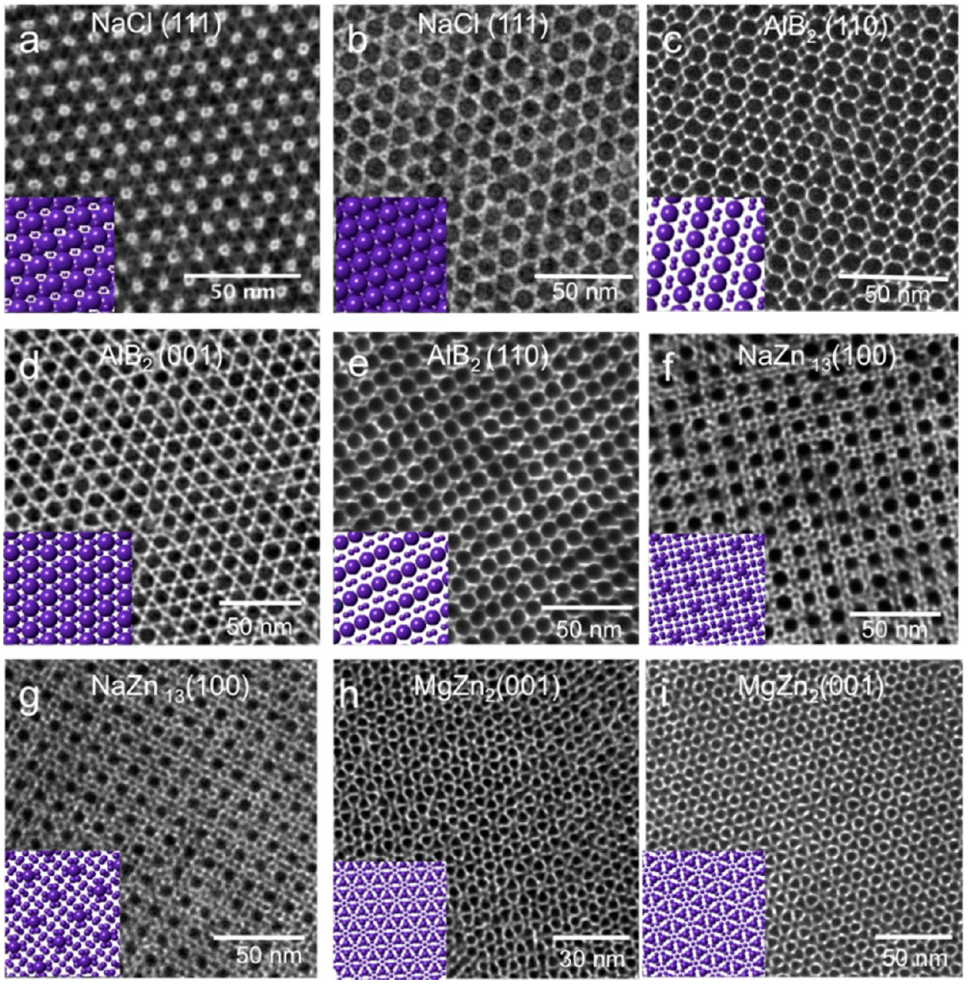

Figure 1. Binary nanocrystal superlattices formed from Ag@OAM in single-ligand systems with $[Ag]_S/[Ag]_L$ = 4: (a) 11.9 nm Ag@OAM and 2.9 nm Ag@OAM, γ_{eff} = 0.42; (b) 11.9 nm Ag@OAM and 3.7 nm Ag@OAM, γ_{eff} = 0.44; (c) 9.6 nm Ag@OAM and 3.7 nm Ag@OAM, γ_{eff} = 0.52; (d) 8.2 nm Ag@OAM and 2.9 nm Ag@OAM, γ_{eff} = 0.55; (e) 8.2 nm Ag@OAM and 3.7 nm Ag@OAM, γ_{eff} = 0.58; (f) 8.2 nm Ag@OAM and 3.7 nm Ag@OAM, γ_{eff} = 0.58; (g) 7.5 nm Ag@OAM and 3.7 nm Ag@OAM, γ_{eff} = 0.64; (h) 5.5 nm Ag@OAM and 3.7 nm Ag@OAM, γ_{eff} = 0.79; (i) 7.5 nm Ag@OAM and 5.5 nm Ag@OAM, γ_{eff} = 0.81.

result of previous observation of such aperiodic structure.[25] Figure 3g shows that the QC superlattices grow through a layer-by-layer process. The domain size of such QC order is as large as several micrometers, as shown in Figure 4. It is of importance to note that the crystal domain boundaries between CaB_6 and QC phase are observed, as shown in Figure 3f, and are in agreement with the reported growth mechanism based on entropic force.[25] It is also worth noting that, to the best of our knowledge, this is the first demonstration on QC ordering from a single type of material (Ag). Similar experiments were carried out by changing the relative concentration $[Ag]_S/[Ag]_L$ from 2 to 10 while keeping the γ_{eff} = 0.42; QC ordered superlattices were obtained for $2 \leq [Ag]_S/[Ag]_L \leq 4$. In the case of $[Ag]_S/[Ag]_L$ = 10, only CaB_6 and single-component superlattices were produced (Table 3).

In view of the remarkable differences in crystal structures observed in those conditions and by comparison with binary systems made of nanocrystals coated with the same ligand, the

DOI: 10.1021/jacs.5b09959
J. Am. Chem. Soc. 2015, 137, 14773−14784

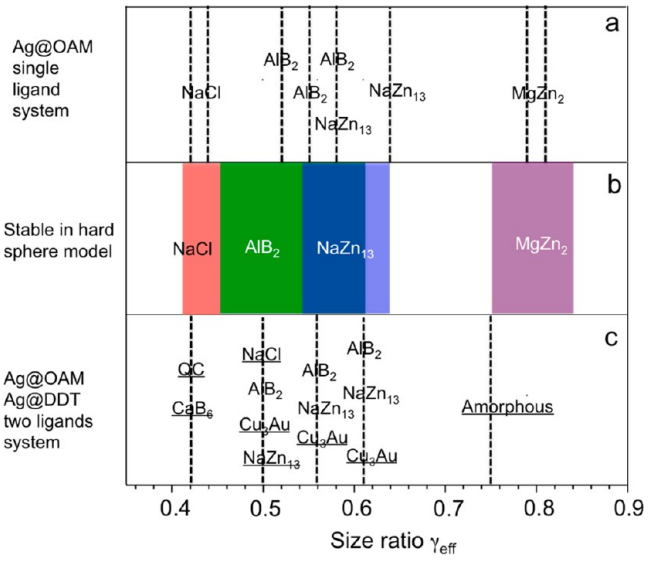

Figure 2. Various binary structures formed: (a) single-ligand system (Ag@OAM); (b) hard-sphere theoretical predictions; (c) two ligands (Ag@OAM) and (Ag@DDT) system.

phase diagram was extended and rebuilt for large and small nanocrystals stabilized by two distinct coating agents. The size of Ag@OAM was increased from 5.5 to 11.9 nm, whereas that of Ag@DDT remained equal to 4 nm. This induced a change in the γ_{eff} values from 0.42 to 0.75. The total Ag concentration remained unchanged (1×10^{-6} M), and the relative concentration $[Ag]_S/[Ag]_L$ evolved from 2 to 10. Upon increasing γ_{eff} to 0.50, various phases appeared, including NaCl, AlB_2, Cu_3Au, and $NaZn_{13}$ structures, as presented in TEM images in Figure 5 and summarized in Table 3. It is worth noting that AlB_2, NaCl, and $NaZn_{13}$ phases are still present in these conditions. According to theoretical calculations based on the hard-sphere model (Figure 2b), AlB_2 is the expected product, whereas the other structures, such as NaCl, Cu_3Au, and $NaZn_{13}$, are not predicted to appear at this size ratio (γ_{eff} = 0.50) (Figure 2c). Furthermore, when the value of γ_{eff} is increased to 0.56 and 0.61, another unstable phase of Cu_3Au structure with a relatively low packing density formed, but was not predicted (see Figure S8, Supporting Information). Furthermore, a $MgZn_2$ structure, which is a highly stable phase in the hard-sphere model, was not produced at large γ_{eff} values (~0.75), and only an amorphous film was observed

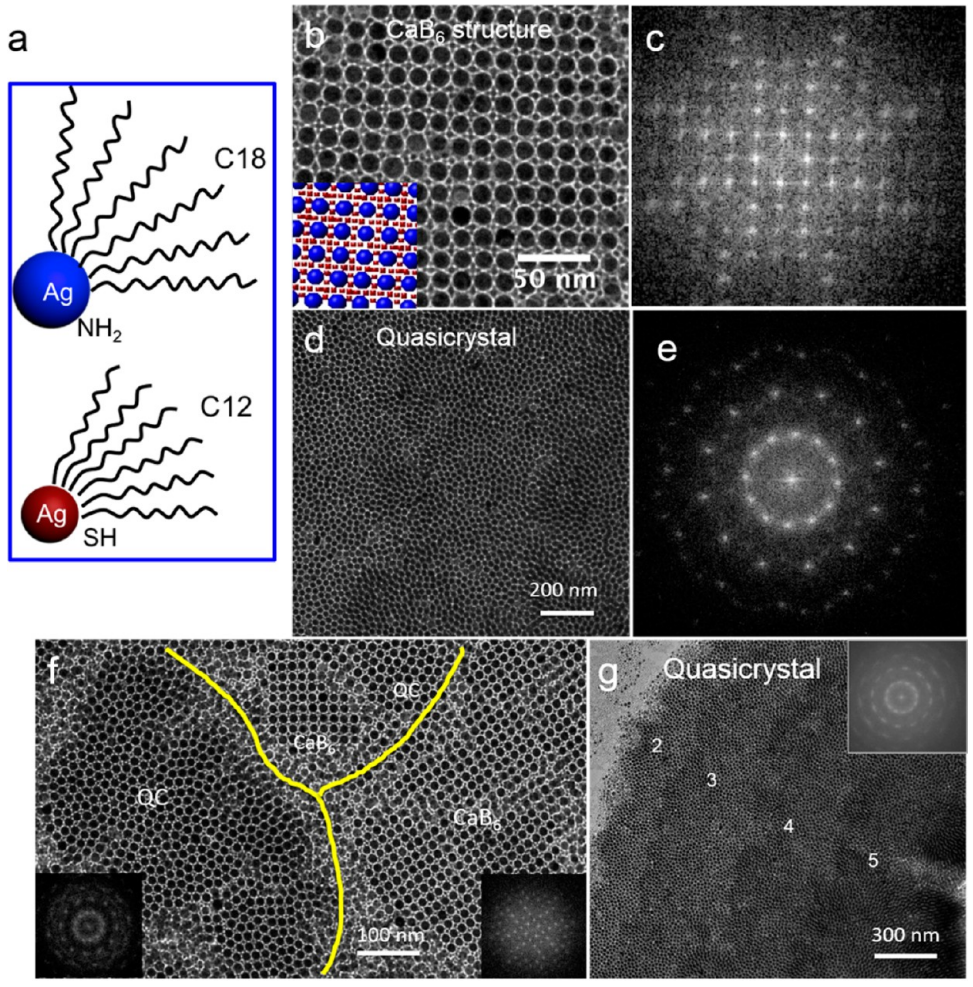

Figure 3. TEM images of binary superlattices formed with 11.9 nm Ag@OAM and 4.0 nm Ag@DDT binary mixtures: (a) scheme of multiple ligand system; (b) TEM images of CaB_6-type binary nanocrystal superlattices with (100) planes parallel to the substrate; (c) corresponding FFT pattern to panel b; (d) TEM images of QC order; (e) corresponding FFT pattern to panel d; (f) mixture of the QC order in binary nanocrystal superlattices and CaB_6-type binary nanocrystal superlattices; (g) TEM images of large-scale QC with layer-by-layer structures (the numbers correspond to the different layers of QC order).

DOI: 10.1021/jacs.5b09959
J. Am. Chem. Soc. 2015, 137, 14773−14784

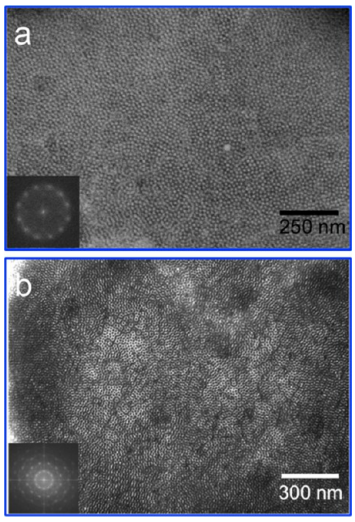

Figure 4. (a) HRSEM (high-resolution scanning electron microscopy) images of QC ordered superlattices formed with 11.9 nm Ag@OAM and 4.0 nm Ag@DDT binary mixtures. (b) Low-magnified TEM images of QC ordered superlattices formed with 11.9 nm Ag@OAM and 4.0 nm Ag@DDT binary mixtures.

instead. These data clearly show that the binary structures produced with two different coating agents markedly differ from the hard-sphere model (Figure 2, parts b and c). Furthermore, the phase diagrams in Figure 2, parts a and c, show marked changes by comparison with the data acquired when using binary systems made of nanocrystals bearing the same coating agents for both small and large components.

The formation of QC order in binary superlattices is of particular interest. Unfortunately, a general fabrication method toward QC order in binary superlattices is still lacking and needs to be developed. Hence, we tried to assess the importance of using two different ligands to coat the nanocrystals on the production of QC and CaB_6 structures. For this purpose, Ag@DDT was replaced by Au@DDT while keeping the same average diameter (4.0 nm) for Au nanocrystals. All other experimental conditions remained unchanged ($[Au]_S/[Ag]_L = 4$; $\gamma_{eff} = 0.41$). In those conditions, CaB_6 and dodecahedral QC structures are clearly observed (Figure 6) and are consistent with the results obtained from the Ag@OAM + Ag@DDT binary system with a similar γ_{eff} value. However, the sizes of the crystal domains of both CaB_6 and dodecahedral QC structures produced are smaller than those of the Ag@OAM + Ag@DDT binary system. This can be attributed to stronger interactions between Au atoms and SH− headgroup than those between SH− and Ag atoms. From these data one can assume that the production of QC order in binary superlattices relies on the presence of small and large nanocrystals coated by two different ligands in the binary systems. To confirm this claim, this experiment was extended to other types of nanocrystals differing by their sizes and coating agents: 12 nm $CoFe_2O_4$ nanocrystals coated with oleic acid (OA) and Ag nanocrystals either coated with oleylamine (Ag@OAM) or with dodecanethiol (Ag@DDT) characterized by an average diameter of 3.7 and 4 nm, respectively, were used. Figure 7 shows binary systems of $CoFe_2O_4$@OA + Ag@OAM (Figure 7a−c) and of $CoFe_2O_4$@OA + Ag@DDT (Figure 7d−f). The TEM image in Figure 7b shows a periodic (3^2.4.3.4) Archimedean tiling. The corresponding FFT pattern (Figure 7b, inset) indicates a 4-fold rotational symmetry in the case of $CoFe_2O_4$@OA and 3.7 nm Ag@OAM binary mixture.[25,26] In addition, dodecagonal QC structures and AlB_2-type structures can also be observed in Figure 7c. In the case of the $CoFe_2O_4$@OA + Ag@DDT binary system, CaB_6-type and dodecagonal QC structures are observed (Figure 7, parts e and f). Hence, in both cases CaB_6-type and dodecagonal QC structures are observed instead of the NaCl phase predicted from the hard-sphere model at this size ratio. This unambiguously demonstrates that the use of two different coating agents for small and large nanocrystals induces the formation of both CaB_6-type and dodecagonal QC structures. Here the alkyl chain lengths (OA and OAM) are similar (C_{18}) with a double bond at the C_9 position for both ligands. However, the interactions between the coating agent polar head groups and the surface atoms of the nanocrystals markedly differ: OA is covalently attached to Co or Fe atoms,[27] whereas OAM is weakly associated with the Ag surface atoms.[28] This clearly shows that coating agent interactions, both in terms of head groups−surface atoms bond strength and the length of the alkyl chains, are important in the QC formation, as observed with Ag@OAM/Ag@DDT and Ag@OAM/Au@DDT (C_{18}/C_{12}).

A careful survey of the literature shows that the formation of either CaB_6 or QC structure in binary superlattices is obtained with nanocrystals having two different coating agents. This was observed for Fe_2O_3@OA + Au@DDT, Fe_3O_4@OA + Au@DDT, and PbS@OA + Pd@DDT binary systems (those data are summarized in Table S1).[25,26,29] This corroborates our findings stating that, in order to produce either CaB_6 or QC structures in binary superlattices, the small and large nanocrystals must be coated by two different coating agents. Note that the length of the ligand used for the formation of QC structure is different from C_{12} DDT to C_{18} OA. We stress that the ligand length difference is not required for the formation of QC structure; even though formation of QC structures was observed while using C_{12} DDT to C_{18} OA, they were also present in the case of 12 nm $CoFe_2O_4$@OA and 3.7 nm Ag@OAM.

The above results unambiguously show that surface coating agents can play a pivotal role in the formation of binary nanocrystal superlattices. In single-ligand binary systems, the resulting binary structures fit well the phase diagrams based on a hard-sphere model. However, divergences emerge when two different coating agents are used, and the resulting binary structures, such as the QC phase, cannot be predicted from the same phase diagrams. Let us consider the various factors responsible for the formation of these binary structures:

1. Presence of Additional Surfactant Molecules. Previous studies pointed out that the addition of a relatively large amount of surfactant could induce surface electrical charges on nanocrystals, even in nonpolar solvents. They may play a role in the binary assemblies by creating electrostatic interactions.[13,30] As mentioned above, the nanocrystals were washed several times to remove all residual surfactant molecules (OAM and DDT). The efficiency of this washing process and the removal of the residual surfactant molecules was assessed by considering the surface plasmon resonance (SPR) of a colloidal solution composed of a mixture of 11.9 nm Ag@OAM and 4 nm Ag@DDT nanocrystals in the same ratio as the one used to produce the binary structures shown above. The SPR absorption of the colloidal solution produced without washing markedly changed by comparison to that of the nanocrystals washed three times (Figure S9, Supporting Information). The SPR bandwidth of washed nanocrystals is very narrow

DOI: 10.1021/jacs.5b09959
J. Am. Chem. Soc. 2015, 137, 14773−14784

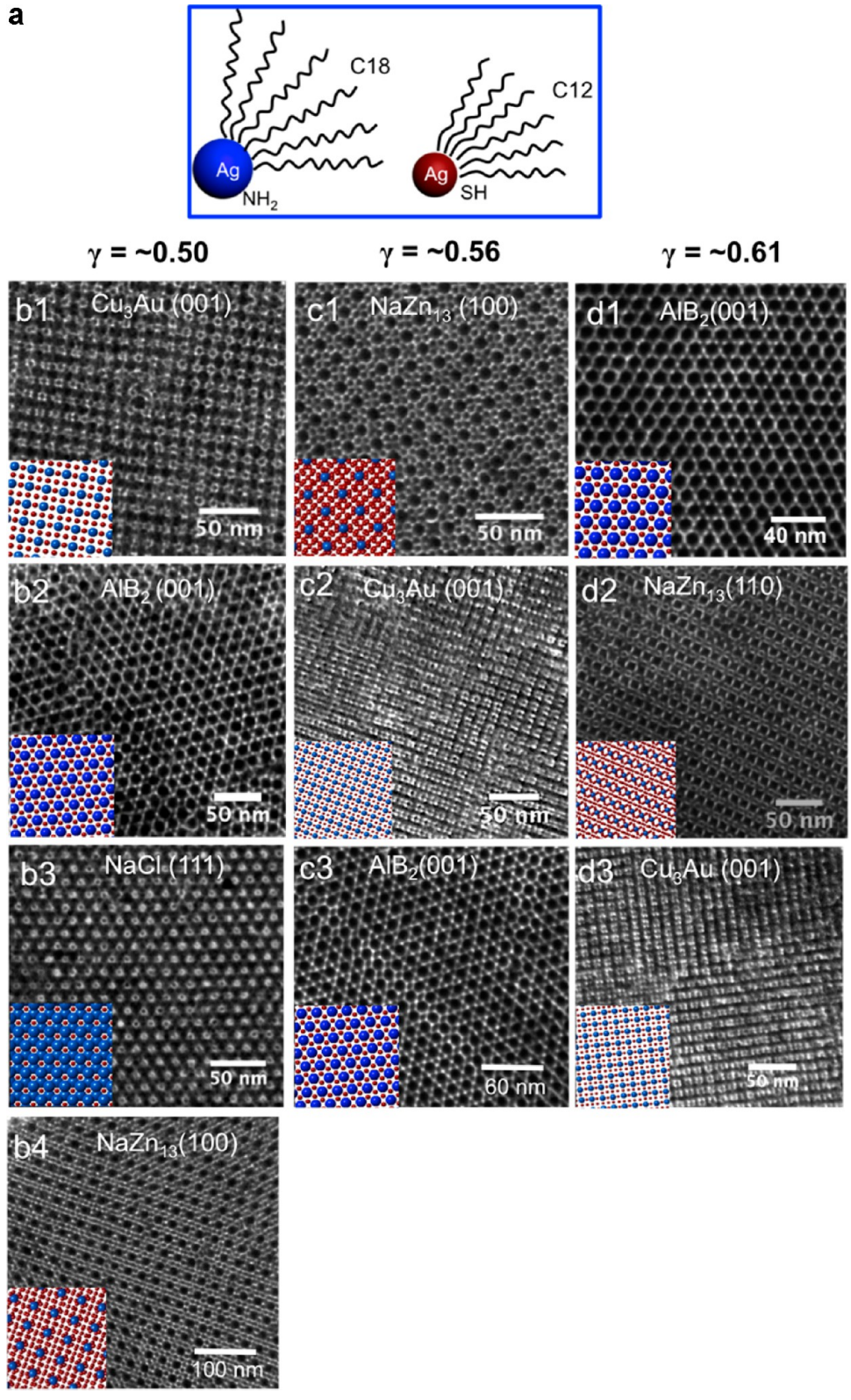

Figure 5. TEM images of binary superlattices formed with Ag@OAM and Ag@DDT binary mixtures: (a) scheme of multiple ligand system; (b1−b4) TEM images of Cu_3Au, AlB_2, NaCl, and $NaZn_{13}$ phases with $\gamma_{eff} \approx 0.50$; (c1−c3) TEM images of $NaZn_{13}$, Cu_3Au, and AlB_2 phases with $\gamma_{eff} \approx 0.56$; (d1−d3) TEM images of $NaZn_{13}$, AlB_2, and Cu_3Au phases with $\gamma_{eff} \approx 0.61$. Insets in all figures are the corresponding crystal models, respectively.

compared to that obtained without the washing process. This well-known effect is due to the presence of the excess ligand in the colloidal solution inducing flocculation of the Ag nanocrystals with a significant color change and a red-shift in the SPR absorption band. In our system, the residual surfactant molecules have been effectively minimized by multiple-step

DOI: 10.1021/jacs.5b09959
J. Am. Chem. Soc. 2015, 137, 14773−14784

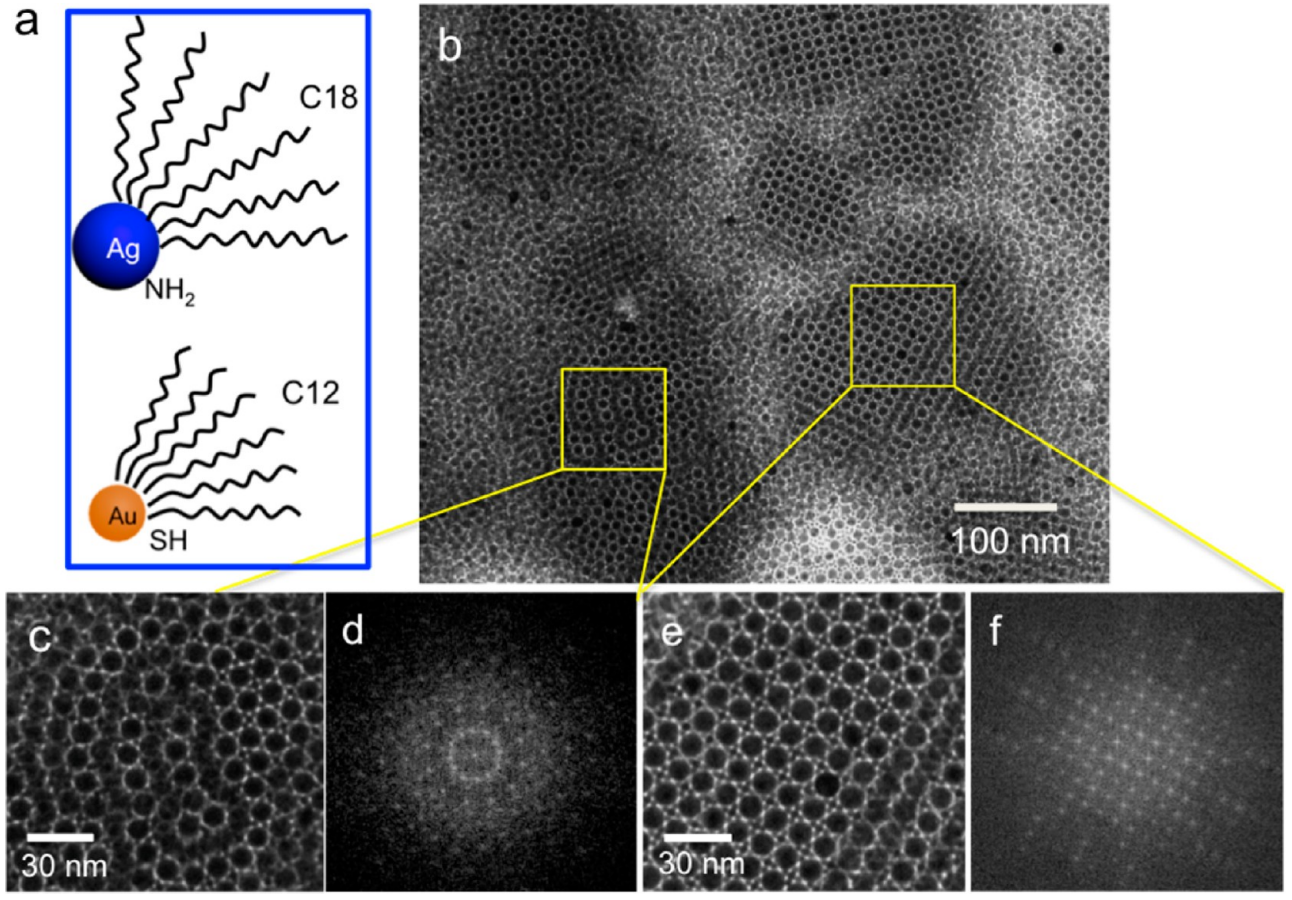

Figure 6. TEM images of binary nanocrystal superlattices from Au−Ag binary mixtures produced with $[Au]_S/[Ag]_L = 4$: (a) scheme of multiple ligands system, 11.9 nm Ag@OAM and 4 nm Au@DDT; (b) low magnification of TEM images of QC superlattices and CaB_6-type superlattices; (c and e) magnification of the area of panel b; (d and f) corresponding FFT pattern of panels c and e.

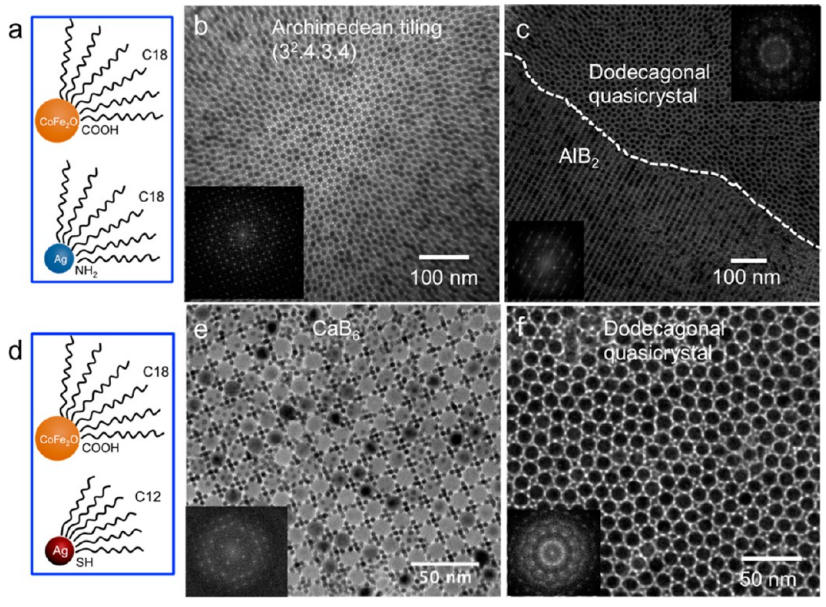

Figure 7. (a) Scheme of multiple ligands system: $CoFe_2O_4$@OA and Ag@OAM; (b and c) TEM image of the binary nanocrystal superlattices formed with 12.0 nm $CoFe_2O_4$@OA and 3.7 nm Ag@OAM binary mixtures with $[Ag]_S/[CoFe_2O_4]_L = 4$; (d) schematic information on multiple ligands system $CoFe_2O_4$@OA and Ag@DDT; (e and f) TEM image of the binary nanocrystal superlattices formed with 12.0 nm $CoFe_2O_4$@OA and 3.7 nm Ag@DDT binary mixtures with $[Ag]_S/[CoFe_2O_4]_L = 4$.

washing before self-assembly experiments. The existence of electrical charges (either positive or negative) is related to the presence of large excess of the ligand. Otherwise, this type of colloidal solution is usually neutral.[15] This indicates that the

DOI: 10.1021/jacs.5b09959
J. Am. Chem. Soc. 2015, 137, 14773−14784

Coulombic interaction cannot be the main force involved in the present binary system. Besides, our recent studies demonstrated that magnetic forces could play a role during the evaporation-induced binary-assembly process. However, only one example of this effect has been reported, in which ferromagnetic nanocrystals were involved.[31]

2. Influence of the van der Waals Interactions. A recent simulation has shown that interactions between metal nanocrystals are strong and that the pair potential that exceeds the thermal energy (k_BT) could play a major role during the assembly of binary nanocrystal superlattices.[14] The Hamaker constant of the various nanocrystals used in this study (Ag, Au, or $CoFe_2O_4$) is different for each material, and the nanocrystal's sizes and the coating agents also differ from one binary system to another. This indicates that, even though the van der Waals interactions play a role, other forces also have to be taken into account.

3. Role of the Ligands in the Nanocrystal Superlattices. Here, both the flexibility and the specific interactions of the ligands head groups with the nanocrystal surface atoms have to be taken into account. In a recent paper,[32] it was pointed out that deformability of the coating layer that is attributed to the change in local coordination environment plays an important role in the packing mode of binary nanocrystal superlattices. Moreover, the specific coordination environment of the nanocrystals is mainly determined by its softness parameter $\chi = L/R$, where L is the thickness of the coating layer and the R the radius of the inorganic core.[33] For single-component nanocrystals, low softness ($\chi < 0.7$), the nanocrystals behave as hard spheres and form close-packed assemblies with face-centered cubic (fcc) symmetries. In contrast, for nanocrystals with a softer ligand shell, $\chi > 0.7$, the interdigitation between the ligands of nanocrystals occurs at longer range, apparently favoring more open body-centered cubic (bcc) structures with lower packing fractions. However, the softness of the organic layer alone cannot account for the results obtained above. For instance, both 11.9 nm Ag@OAM and 12.0 nm $CoFe_2O_4$@OA have a similar softness parameter χ, equal to ~0.4. Consequently, 11.9 nm Ag@OAM/3.7 nm Ag@OAM (Figure 1b) and 12 nm $CoFe_2O_4$@OA/3.7 nm Ag@OAM (Figure 7) binary mixtures are expected to have similar crystalline structures. However, comparison between Figure 1b and Figure 7 clearly shows marked differences: with 11.9 nm Ag@OAM/3.7 nm Ag@OAM mixtures, NaCl-type binary structures are produced, whereas various structures such as QCs, Archimedean tiling structure, and AlB_2-type binary structures are observed with 12 nm $CoFe_2O_4$@OA/3.7 nm Ag@OAM nanocrystals.

4. Role of the Substrate and Evaporation Time. In the experiments described above, the substrate is a TEM grid covered by a carbon film and the time for solvent evaporation is approximately 4 h. We take the 11.9 nm Ag@OAM and 4.0 nm Ag@DDT binary system as an example, while the Ag nanocrystals are dispersed in hexane instead of toluene. These two colloidal solutions were mixed ($V_{4.0nmAg@DDT}/V_{11.9nmAg@OAM} = 4$), and 20 μL (instead of 40 μL as described above) of the colloidal solution was deposited on an ethylene glycol (EG)−air interface, where EG is used as a perfect substrate.[34] After the evaporation of carrier solvent, an interfacial film was formed and transferred to a carbon-coated TEM grid by using a tungsten ring. The results are shown in Figure 8, which exhibit a NaCl-type binary structure, similar to what was observed shown in Figure 1 when using nanocrystals

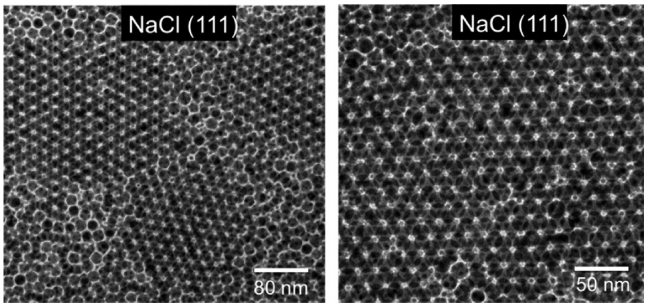

Figure 8. TEM images of superlattices assembled with 11.9 nm Ag@OAM and 4.0 nm Ag@DDT grown on air−EG (ethylene glycol) surface.

bearing the same ligands. In such experimental condition, the solvent evaporation time is drastically decreased from 4 h (toluene) to 5 min (hexane). Besides, inclusion of EG molecules into the nanocrystals' "soft shell" occurs. Such process is expected to enable "locking" of the coating agent molecules at the interface, as inferred by previous studies[35] that the optical properties of Ag nanocrystals deposited on EG interface markedly change compared to those of the same assemblies on a glass wafer. From these data it is speculated that the influence of ligands on the self-assembly of binary mixtures is probably a kinetically controlled process.

Previous study carried out on the optical properties of silver nanocrystals shows that, for a given nanocrystal size, the SPR band position depends on the bonding strength between the ligand and the nanocrystal surface atoms.[35] For instance, the SPR spectra of 4 nm Ag nanocrystals coated with OAM and DDT dispersed in toluene are centered at 418 and 431 nm, respectively. Replacing OAM by DDT as coating agent induces a red-shift of the SPR band. The SPR of 11.9 nm Ag nanocrystals coated with OAM is centered at 411 nm (inset in Figure 9). When 11.9 nm Ag@OAM and 4 nm Ag@DDT toluene solutions are mixed, the SPR spectrum of this solution

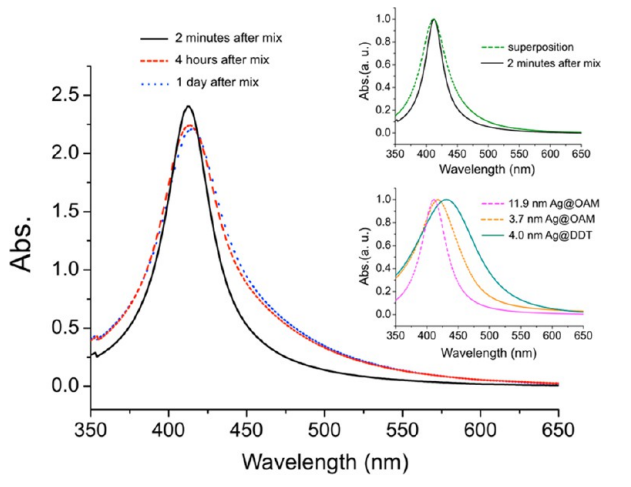

Figure 9. Surface plasmon resonance (SPR) spectra of mixed Ag nanocrystals colloidal solution at different times after mixing. Inset 1 (top) is the normalized SPR spectrum of mixed Ag nanocrystals colloidal solution 2 min after mixing (black solid line) and spectra superposition of 11.9 nm Ag@OAM and 4.0 nm Ag@DDT (green dashed line); inset 2 (bottom) is the normalized SPR spectra of 11.9 nm Ag@OAM (pink dashed line), 3.7 nm Ag@OAM, and 4.0 nm Ag@DDT.

DOI: 10.1021/jacs.5b09959
J. Am. Chem. Soc. 2015, 137, 14773−14784

Scheme 1. (i and ii) Representation of the Equilibriums of the Bonding of Nanocrystal−Ligand with Different Sizes and Different Coating Agents by Adsorption and Desorption Kinetic Constants, k_a and k_d; (iii) Representation of Ligand Exchange between Nanocrystals with Different Surface Coatings

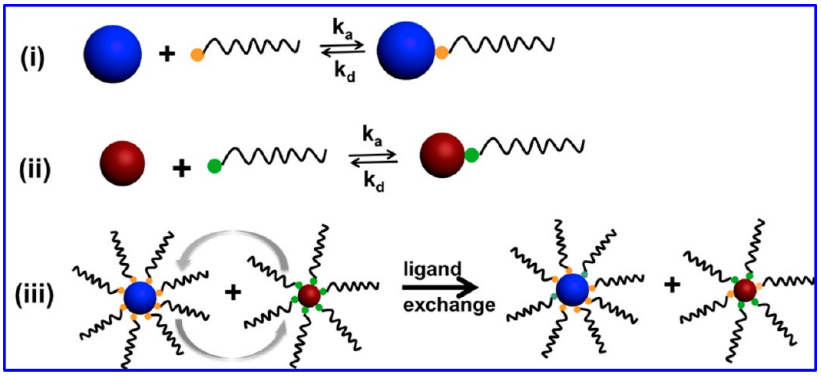

shows a well-defined peak with a very narrow bandwidth that is smaller than the superposition of the spectra of corresponding large and small nanocrystals (inset in Figure 9). Furthermore, a slight red-shift and a broadening in the SPR band are observed after 4 h (Figure 9). It can be attributed to ligand exchange between 11.9 nm Ag@OAM and 4 nm Ag@DDT. It is pointed out that no precipitation is observed here. From these data we propose that ligand exchange can also take place during the self-assembly of binary mixtures when the carrier solvent evaporates.

The deposition process lasts for approximately 4 h at 35 °C. During this continuous drying process, dynamic ligand adsorption/desorption on the nanocrystal surface takes place in the colloidal solution, regardless of the different bonding efficiencies between nanocrystal cores and the coating agents from one system to another. This bonding between each nanocrystal core and coating agent can be described by its adsorption and desorption equilibrium constant, K, and the adsorption and desorption kinetic constants, k_a and k_d, respectively. $K = k_a/k_d$, where K represents the thermodynamics of a nanocrystal−ligand system and k_a and k_d depict the dynamic feature of the system.[36] The K constant is generally associated with the adsorption/desorption equilibrium by the Arrhenius equation.

$$\Delta G = RT \ln K = RT \ln(k_a/k_d)$$

For binary systems with the same coating agent in which QC or CaB_6 structures are not observed, such as Ag@OAM, it is assumed in first approximation that the adsorption and desorption kinetic constants k_a and k_d are kept constant and are independent of the nanocrystals' sizes.[36] Thus, the thermodynamic term K in the binary system remains constant. Hence, the assembly of binary nanocrystal mixtures with the same coating agent is mainly determined by their effective size ratios. At the equilibriums state, the ligand coverage on the nanocrystal surface remains constant. Thus, the nanocrystals coated with the same capping ligand (Ag@OAM, for example) can be considered as hard spheres despite the fact that ligands interdigitation takes place between neighboring nanocrystals. This explains the agreement between the experimental data and the hard-sphere model obtained above with Ag nanocrystals bearing the same coating agent (OAM).

For binary system with two different kinds of coating agents, the thermodynamic constant K differs from each type of nanocrystal. For instance, the thermodynamic $K_{Ag@OAM}$ for Ag@OAM differs from the $K_{Ag@DDT}$ for Ag@DDT. It is known that, for nanocrystals of similar size, the SPR band of Ag@DDT is red-shifted compared to that of Ag@OAM (inset in Figure 9). This was attributed to stronger bonding of thiol head groups (−SH) than that of amine-terminated ligands onto metallic surfaces. During solvent evaporation, one can assume that ligand exchange processes take place as illustrated in Scheme 1. Complete evaporation of the carrier solvent provides sufficient time for this ligand exchange process to occur in the colloidal solution. During the formation of nanocrystal superlattices, the system must pay a large energetic penalty to enable the ligand exchange process, which can affect the thermodynamics of the assembly of binary nanocrystal superlattices during solvent evaporation. Thus, the formation of a superlattice with lower packing density may be favored kinetically because the required energetic penalty is smaller than that of a denser structure.[37] In other words, a binary structure is likely to be in a kinetically trapped state at a local free energy minimum in spite of its lower packing density. This supposition is supported by the observation of NaCl structure when the evaporation time decreases and the ligand exchange process is partially prevented by inclusion of EG molecules into the nanocrystals' "soft shell", as shown in Figure 8. As a result, binary structures such as CaB_6, QC, and Cu_3Au phases with lower packing densities, and that are absent in hard-sphere systems, can be produced in nanoscale binary systems. These data implies that the ability to control the surface chemistry in binary systems may provide another efficient way to control the crystal structures of binary nanocrystal superlattices.

■ CONCLUSIONS

Here it is shown that the crystal structures of binary nanocrystal superlattices made from binary mixtures can be predicted from calculated phase diagrams based on a hard-sphere model when using only one coating agent. Four types of binary structures, NaCl, AlB_2, $NaZn_{13}$, and $MgZn_2$, can be produced; they are driven purely by entropic considerations. When two different coating agents are used to coat the nanocrystals in a binary system, the phase diagram observed markedly changes with the appearance of various phases such as QC, CaB_6, and Cu_3Au. A ligand exchange process is believed to be responsible for the interparticle interactions between neighboring nanocrystals, resulting in diversity in binary nanocrystal superlattices including some structures with lower packing density. The formation of these structures is probably because of a kinetically

DOI: 10.1021/jacs.5b09959
J. Am. Chem. Soc. 2015, 137, 14773−14784

trapped state at a local free energy minimum. Our findings are of particular importance for the design of novel 3D metamaterials from the numerous colloidal nanocrystals libraries available now.

EXPERIMENTAL SECTION

Materials. Silver nitrate (99.9%), methanol (99.8%), *o*-dichlorobenzene (99%), oleylamine (70%), oleic acid (90%), iron(III) chloride hexahydrate (Sigma-Aldrich, 97%), ethylene glycol (Sigma-Aldrich, 99.8%), 1-octadecene (Aldrich, 90%), hexane (Sigma-Aldrich, 95%), dodecanediol (99%), dodecanethiol (99%), and *tert*-butylamine (97%) were purchased from Sigma, chloro(triphenylphosphine)gold (98%) was purchased from STREM, toluene (98%) was from Riedel de Haen, and ethanol (99.8%) was from Prolabo. All reagents were used as received without further purification.

Apparatus. Transmission electron microscopy images were obtained on a JEOL JEM 1011 (100 kV). High-resolution scanning electron microscopy (HRSEM) images were obtained on a Hitachi Su-70 instrument. Optical absorption measurements were carried out on a Varian Cary 5000 spectrophotometer using 1 mm cuvettes.

Synthesis of Nanocrystals. The 3.7 and 5.5 nm Ag nanocrystals were synthesized by a hot injection method, and oleylamine was used as a coating agent, as described elsewhere.[28] For the synthesis of 2.9 nm Ag nanocrystals, 100 μL of oleic acid and 1 mL of oleylamine were added to control the size. The excess oleic acid was washed five times through ethanol−toluene cycles, and an additional 50 μL of oleylamine was added during the washing cycles. The 7.5, 8.2, 9.6, and 11.9 nm Ag nanocrystals were synthesized by a one-pot method, also using oleylamine as coating agent.[38] Thiol-coated 4 nm Ag nanocrystals were prepared by the reverse micelles method.[39] All the nanocrystals can be seen in the TEM images in Figure S1. All the nanocrystals were dispersed in toluene and exhibited a size distribution below 10% (Table 1). Synthesis of 4.0 nm Au nanocrystals coated with dodecanethiol was carried out according to the revised Stucky's method.[40,41] In addition, 12 nm $CoFe_2O_4$ nanocrystals coated with oleic acid were produced from thermal decomposition of a mixture of cobalt oleate and iron oleate as published elsewhere.[42] The synthesis details and the TEM images of Au nanocrystals and $CoFe_2O_4$ are shown in Supporting Information (Figure S2).

Superlattices Formation. Self-assemblies of binary colloidal solutions were carried out using an experimental setup previously described,[43] and the temperature was set to 35 °C in the present study. Carbon-coated copper TEM grids were used as the substrate for depositions of superlattices. The grids were placed inside a glass vial with inner diameter of ∼4 mm. Then 40 μL of solution containing a binary mixture of nanocrystals with the desired nanoparticle ratios was injected into the glass vial while keeping the overall particle concentration constant at $\sim 1 \times 10^{-6}$ M. Concentrations of the Ag nanocrystals were estimated by weighing the mass of the final product. The mixed colloidal solution was evaporated under N_2 flow.

ASSOCIATED CONTENT

Supporting Information

The Supporting Information is available free of charge on the ACS Publications website at DOI: 10.1021/jacs.5b09959.

TEM images of the nanocrystals used for assembly process and the additional TEM images of binary assemblies (PDF)

AUTHOR INFORMATION

Corresponding Author

*mppileni@orange.fr

Notes

The authors declare no competing financial interest.

ACKNOWLEDGMENTS

The research leading to these results has been supported by an advanced grant of the European Research Council under Grant 267129. J.W. thanks the China Scholarship Council for financial support.

REFERENCES

(1) Sanders, J. V. *Nature* **1964**, *204*, 1151−1153.
(2) Allpress, J. G.; Sanders, J. V. *Surf. Sci.* **1967**, *7*, 1−25.
(3) Bartlett, P.; Ottewill, R. H.; Pusey, P. N. *Phys. Rev. Lett.* **1992**, *68*, 3801−3804.
(4) Eldridge, M. D.; Madden, P. A.; Frenkel, D. *Nature* **1993**, *365*, 35−37.
(5) Ohara, P. C.; Leff, D. V.; Heath, J. R.; Gelbart, W. M. *Phys. Rev. Lett.* **1995**, *75*, 3466−3469.
(6) Korgel, B. A.; Fullam, S.; Connolly, S.; Fitzmaurice, D. *J. Phys. Chem. B* **1998**, *102*, 8379−8388.
(7) Murray, C. B.; Kagan, C. R.; Bawendi, M. G. *Annu. Rev. Mater. Sci.* **2000**, *30*, 545−610.
(8) Henry, A. I.; Courty, A.; Pileni, M. P.; Albouy, P. A.; Israelachvili, J. *Nano Lett.* **2008**, *8*, 2000−2005.
(9) Murray, C. B.; Kagan, C. R.; Bawendi, M. G. *Science* **1995**, *270*, 1335−1338.
(10) Pileni, M. P. *Acc. Chem. Res.* **2007**, *40*, 685−693.
(11) Choi, J. J.; Bealing, C. R.; Bian, K.; Hughes, K. J.; Zhang, W.; Smilgies, D.-M.; Hennig, R. G.; Engstrom, J. R.; Hanrath, T. *J. Am. Chem. Soc.* **2011**, *133*, 3131−3138.
(12) Chan, H.; Demortiere, A.; Vukovic, L.; Kral, P.; Petit, C. *ACS Nano* **2012**, *6*, 4203−4213.
(13) Shevchenko, E. V.; Talapin, D. V.; Kotov, N. A.; O'Brien, S.; Murray, C. B. *Nature* **2006**, *439*, 55−59.
(14) Evers, W. H.; Nijs, B. D.; Filion, L.; Castillo, S.; Dijkstra, M.; Vanmaekelbergh, D. *Nano Lett.* **2010**, *10*, 4235−4241.
(15) Bodnarchuk, M. I.; Kovalenko, M. V.; Heiss, W.; Talapin, D. V. *J. Am. Chem. Soc.* **2010**, *132*, 11967−11977.
(16) Filion, L.; Dijkstra, M. *Phys. Rev. E* **2009**, *79*, 046714.
(17) Vanmaekelbergh, D. *Nano Today* **2011**, *6*, 419−437.
(18) Bodnarchuk, M. I.; Shevchenko, E. V.; Talapin, D. V. *J. Am. Chem. Soc.* **2011**, *133*, 20837−20849.
(19) Shevchenko, E. V.; Talapin, D. V.; Murray, C. B.; O'Brien, S. *J. Am. Chem. Soc.* **2006**, *128*, 3620−3637.
(20) Bodnarchuk, M. I.; Erni, R.; Krumeich, F.; Kovalenko, M. V. *Nano Lett.* **2013**, *13*, 1699−1705.
(21) Chen, Z.; O'Brien, S. *ACS Nano* **2008**, *2*, 1219−1229.
(22) Parthe, E. *Z. Kristallogr.* **1961**, *115*, 52−79.
(23) Yang, Z.; Wei, J.; Pileni, M. P. *Chem. Mater.* **2015**, *27*, 2152−2157.
(24) Saunders, A. E.; Korgel, B. A. *ChemPhysChem* **2005**, *6*, 61−65.
(25) Talapin, D. V.; Shevchenko, E. V.; Bodnarchuk, M. I.; Ye, X.; Chen, J.; Murray, C. B. *Nature* **2009**, *461*, 964−967.
(26) Ye, X.; Chen, J.; Murray, C. B. *J. Am. Chem. Soc.* **2011**, *133*, 2613−2620.
(27) Wu, N.; Fu, L.; Su, M.; Aslam, M.; Wong, K. C.; Dravid, V. P. *Nano Lett.* **2004**, *4*, 383−386.
(28) Wei, J.; Schaeffer, N.; Pileni, M.-P. *J. Phys. Chem. B* **2014**, *118*, 14070−14075.
(29) Bodnarchuk, M. I.; Erni, R.; Krumeich, F.; Kovalenko, M. V. *Nano Lett.* **2013**, *13*, 1699−1705.
(30) Sun, Z.; Luo, Z.; Fang, J. *ACS Nano* **2010**, *4*, 1821−1828.
(31) Yang, Z.; Wei, J.; Bonville, P.; Pileni, M.-P. *J. Am. Chem. Soc.* **2015**, *137*, 4487−4493.
(32) Boles, M. A.; Talapin, D. V. *J. Am. Chem. Soc.* **2015**, *137*, 4494−4502.
(33) Goodfellow, B. W.; Korgel, B. A. *ACS Nano* **2011**, *5*, 2419−2424.
(34) Dong, A. G.; Chen, J.; Vora, P. M.; Kikkawa, J. M.; Murray, C. B. *Nature* **2010**, *466*, 474−477.

DOI: 10.1021/jacs.5b09959
J. Am. Chem. Soc. 2015, 137, 14773−14784

(35) Wei, J.; Schaeffer, N.; Albouy, P.-A.; Pileni, M.-P. *Chem. Mater.* **2015**, *27*, 5614−5621.
(36) Ji, X.; Copenhaver, D.; Sichmeller, C.; Peng, X. *J. Am. Chem. Soc.* **2008**, *130*, 5726−5735.
(37) Nagaoka, Y.; Chen, O.; Wang, Z.; Cao, Y. C. *J. Am. Chem. Soc.* **2012**, *134*, 2868−2871.
(38) Peng, S.; Mcmahon, J. M.; Schatz, G. C.; Gray, S. K.; Sun, Y. *Proc. Natl. Acad. Sci. U. S. A.* **2010**, *107*, 14530−14534.
(39) Courty, A.; Richardi, J.; Albouy, P.-A.; Pileni, M.-P. *Chem. Mater.* **2011**, *23*, 4186−4192.
(40) Zheng, N.; Fan, J.; Stucky, G. D. *J. Am. Chem. Soc.* **2006**, *128*, 6550−6551.
(41) Goubet, N.; Portales, H.; Yan, C.; Arfaoui, I.; Albouy, P. A.; Mermet, A.; Pileni, M. P. *J. Am. Chem. Soc.* **2012**, *134*, 3714−3719.
(42) Bodnarchuk, M. I.; Kovalenko, M. V.; Groiss, H.; Resel, R.; Reissner, M.; Hesser, G.; Lechner, R. T.; Steiner, W.; Schäffler, F.; Heiss, W. *Small* **2009**, *5*, 2247−2252.
(43) Wan, Y. F.; Goubet, N.; Albouy, P. A.; Pileni, M. P. *Langmuir* **2013**, *29*, 7456−7463.

DOI: 10.1021/jacs.5b09959
J. Am. Chem. Soc. 2015, 137, 14773−14784